Transactions of the Korean Nuclear Society Spring Meeting
Jeju, Korea, May 22-23, 2025

Enhanced Corrosion Resistance against Molten Chloride Salt Media Using $MgAl_2O_4$ Conversion Layer: Dynamic Interaction of Porous Alumina with Molten NaCl-$MgCl_2$

Jun Heo, Md Amir Sohel, Dornum Katusiime, and Sung Oh Cho*
Department of Nuclear and Quantum Engineering, Korea Advanced Institute of Science and Technology (KAIST), Daejeon 34141, Korea
**Corresponding author: socho@kaist.ac.kr*

***Keywords: Molten Salt Reactor, Corrosion Resistance, Anodization, Porous Alumina, and $MgAl_2O_4$ Spinel**

1. Introduction

First proposed in the 1950s, molten salt reactors (MSRs) are categorized as fourth-generation nuclear power reactors. Compared to third-generation pressurized reactors, MSRs offer improved thermal efficiency due to their higher operating temperatures (500–750°C), better fuel economy, and enhanced safety due to their lower working pressure and automatic shutdown system[1-3]. At the same time, MSRs enable the downsizing and cost reduction resulting in a promising next-generation nuclear technology. Despite these advantages, material degradation caused by aggressive molten salt coolant remains a significant issue. For MSRs, two main types of molten salt coolants are being considered: salts based on fluoride and chloride. Fluoride salts have been the subject of much research worldwide due to their exceptional heat transfer capabilities, minimal neutron absorption, and good chemical stability. However, because of their affordability and comparable thermophysical characteristics with fluoride, various countries—including ours—have recently turned their attention to chloride salts. Chloride salts are particularly useful for breeding mechanisms, which increases their attractiveness for nuclear applications. The eutectic mixture of NaCl and $MgCl_2$ is a promising option for Molten Chloride Salt Reactors (MCSRs) among different chloride salt compositions, balancing cost-effectiveness and thermal capacity[4]. While pure NaCl-$MgCl_2$ is thermodynamically stable and does not inherently induce corrosion, impurities in the salt, particularly residual water and oxygen, can lead to significant degradation by forming vulnerable oxides and acids that dissolve structural metals[1].

Conventional techniques to mitigate corrosion from molten salts include "alloying" and " redox control"[1]. Alloying improves material performance by adding components that are more resistant to corrosion. However, this approach is expensive and often leads to unpredictable changes in the properties, necessitating careful characterization. Redox control, which involves adding sacrificial elements to maintain a chemically reducing environment, also suffers from high costs and operational complexity. As alternatives, surface coating techniques such as arc ion plating, magnetron sputtering, and thermal spray deposition have lately been studied[1,5,6]. Although these methods can improve corrosion resistance, they are nevertheless limited by adhesion problems, high process complexity, high expense, and geometrical limitations.

In this study, we propose an anodically produced oxide layer as a novel way to enhance corrosion resistance in molten salt environments. Anodization is a cost-effective, scalable, and geometrically versatile technique that provides strong adhesion due to its surface transformation mechanism. Specifically, we are to investigate the formation of a protective $MgAl_2O_4$ spinel oxide layer. This spinel structure has many advantages, including a high melting temperature (~2135°C), good hardness (~16 GPa), high tensile strength (120–300 MPa), and exceptional resistance to chemical attack. Alumina (Al_2O_3) has been extensively studied for corrosion prevention in molten chloride media due to its inherent inertness[7-9]. However, $MgAl_2O_4$ spinel invariably develops as a corrosion product when alumina is exposed to molten salt containing $MgCl_2$[10,11]. Protection is eventually compromised when Mg^{2+} is inserted into the alumina lattice because it causes considerable volumetric expansion, microcracking, and structural instability[10,12]. Thus, deliberately forming a pre-stabilized $MgAl_2O_4$ layer may provide a more robust protective barrier.

Our approach consists of two key steps: (1) anodization to create porous alumina, followed by (2) exposure to molten NaCl-$MgCl_2$ to transform it into $MgAl_2O_4$. As a reactive template for the inclusion of magnesium, porous alumina is created in the first step. To do this, selecting the appropriate anodization material and optimizing process parameters are essential. FeCrAl alloy's high aluminum content, low cost, and high accessibility led to its selection as the base material. Anodization is an electrochemical surface modification process governed by two competing reactions[13]: anodic oxide formation, which is influenced by the electrochemical Gibbs free energy, and oxide dissolution, which depends on electrolyte composition rather than applied energy. By controlling these parameters, the surface oxide composition and structure can be tailored to achieve a porous alumina layer. To facilitate the production of $MgAl_2O_4$, the porous alumina layer is exposed to molten NaCl-$MgCl_2$ in the second step. A dense and stable layer of $MgAl_2O_4$ is created when the salt's magnesium oxide (MgO) and Mg^{2+} ions combine with alumina[14]. Exchange between Mg^{2+} and Al^{3+} is facilitated by the kinetic energy available at high temperatures. The porous structure for stress relaxation encourages the creation of a compact, mechanically stable $MgAl_2O_4$ layer, whereas dense alumina normally cannot tolerate the accompanying volumetric expansion, resulting in cracking and failure.

The factors necessary for the formation of porous alumina and the growth of $MgAl_2O_4$ are precisely explored in this work. Corrosion experiments were performed at 600 °C for 100–500 h to evaluate the protectiveness of the anodized FeCrAl samples compared to bare FeCrAl. The results show that an advantageous protective layer can be formed by utilizing a corrosive environment. This transformation of corrosion threats into protective mechanisms represents a novel strategy for mitigating material degradation in molten salt reactors and other industrial applications involving molten salts.

2. Experimental Section

2.1 Anodization

The working and counter electrode was fully immersed in the electrolyte to apply the voltage during the anodization. For the working electrode, as mentioned earlier, FeCrAl alloy (Fecralloy foil, Goodfellow) was used. The specific composition of the alloy is as follows: Cr: 22.0 wt%, Al: 5.0 wt%, Mn: 0.2 wt%, Si: 0.3 wt%, Y: 0.1 wt%, and Fe: balanced. In the case of counter electrode, Platinum sheets (99.9%) were used. The electrolyte used was composed of Ammonium fluoride (NH_4F), Potassium hydroxide (KOH), and Distilled water (H_2O) with an Ethylene Glycol base. The composition ratio and the applied voltage were later determined after the optimization procedure. Before the anodization, FeCrAl alloy was electropolished in the 10 vol% Perchloric acid ($HClO_4$) + Ethanol bath with 15 V applied for 45 sec. The electropolishing bath was placed in the 15 ℃ water bath to maintain the temperature of the electrolyte. The electropolished samples were, then, sonicated in ethanol and distilled water for 15 min. each. After drying the electropolished samples in the 70 ℃ vacuum oven, samples were finally anodized. Following the ethanol-dipping process for 20 min., anodized samples were heat-treated right away to completely remove the fluorine species from NH_4F and crystallize the anodic layer. For five hours, each sample underwent a vacuum heat-treatment at 500 ℃.

2.2 Corrosion

The corrosion procedure was conducted in the inert atmosphere using a glove box maintaining the H_2O & O_2 under 1 ppm (Fig. 1). The structural materials for the attached furnace were stainless steel 304 including the basket carrying the corrosion crucibles. Alumina (Al_2O_3) crucible was selected for the corrosion procedure having wire fixing holes at the top of the crucible (Fig.1). FeCrAl wire was used for the placement of the anodized samples in the molten salt containing alumina crucible. For the molten chloride salt used for the corrosion test, an eutectic mixture of NaCl and $MgCl_2$ was used. The specific composition for the eutectic mixture was 45.8 mol% for NaCl and 54.2 mol% for $MgCl_2$. The mixture was heated in the following sequence for stabilization and purification: 117 ℃ for 8 h, 180 ℃ for 8 h, 240 ℃ for 2 h, 400 ℃ for 1 h, and 600 ℃ for 10 h[15]. The molten salt was then immediately poured into the crucible and ground. Using the NaCl-$MgCl_2$ eutectic mixture powder, the molten salt corrosion tests were conducted for 100 to 500 h.

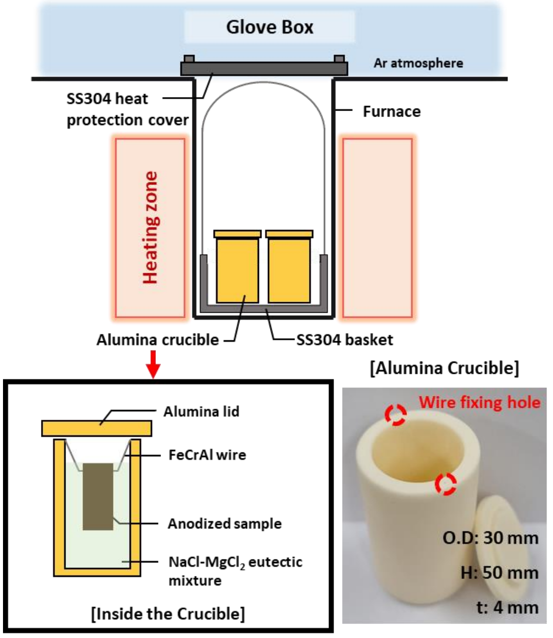

Fig. 1. Schematic of molten salt corrosion system: glove box with inert atmosphere & alumina crucible corrosion kit

2.3 Characterization

All the surface and the cross-section view of the samples were characterized using a Scanning Electron Microscope (SEM, SU500 Hitachi) with Energy-Dispersive X-ray Spectroscopy (EDS). The close cross-sectional view of anodized samples was examined using a Transmission Electron Microscope (TEM, Spectra Ultra Thermofishier). A deeper understanding of the anodic layer composition was achieved through X-ray

Photoelectron Spectroscopy (XPS, Axis-Supra, Kratos) in the depth direction.

3. Results & Discussion

The Anodization process is composed of two significant reactions: anodic formation & chemical dissolution. The anodic formation reaction of a single metal is mainly affected by the oxide forming Gibbs free energy determined by the potential input. On the other hand, the chemical dissolution reaction is affected by the chemical composition of the electrolyte used. By controlling those two aspects, various types of anodic layers can be generated. In the case of alloy, a variety of metals are combined in the lattice. Then the energy input and the chemical composition would affect the types and structures of the generated anodic layer in more complex ways. Therefore, firstly, the optimized chemical composition for producing a porous structure can be tested. After, with that porous structure, the energy input control can be conducted to form the alumina on the surface mainly

3.1 Anodization: Structural control

The electrolyte was composed of NH_4F, KOH, H_2O, and Ethylene glycol. Because each component has a specific role in the anodization process, structure characterization was conducted by controlling the ratio. First of all, the ethylene glycol base was utilized to stabilize and slow down the aggressive electrochemical reactions owing to its high viscous properties. The fluorine species from NH_4F are the main chemical reactants that generate pores in the oxide layer[16]. In the case of KOH, by providing the OH- in the electrolyte, it can play the role of oxygen source for oxide forming reaction. However, the excessive amount of OH- can cause pH control problems which can significantly dissolve the oxide layer[17]. The H_2O also plays a significant role as an oxygen-providing source. At the same time, however, it can also dissolve the oxide layer with an excessive ratio[18]. To verify the effect of each component, the component ratio was modified from 0.01 M to 0.1 M, and the structures were characterized as shown in Fig.2. Increase in the porosity can be characterized by increasing the amount of NH_4F amount. In the case of KOH, dissolution, and oxidation behavior were both revealed. By increasing the amount of H_2O in the electrolyte, the dissolution rate was increased and at the same time, the amount of oxidation was also increased showing a higher atomic percentage of oxygen.

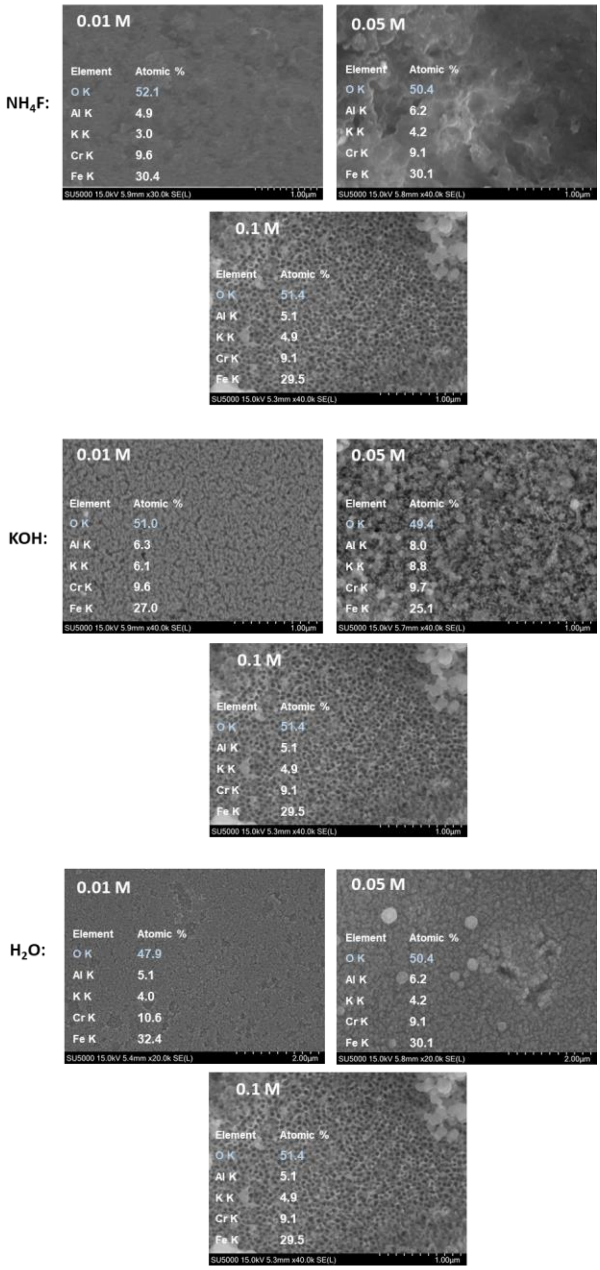

Fig. 2. Surface SEM images with different ratios of NH_4F, KOH, and H_2O factors

From the characterization, 0.1 M of NH_4F + 0.1 M of KOH + 0.1 M of H_2O + Ethylene glycol was the best condition considering the porous structure.

3.2 Anodization: Manipulation of oxide composition

The anodic formation electrochemical reaction is an additional aspect of anodization. Because the energy input affects the Gibbs free energy of oxide forming each metal in the alloy, the composition of the generated oxide layer may be controlled by adjusting the applied potential. Four potential inputs (20, 30, 60, and 80 V) were evaluated using the porous structure provided by the previously indicated chemical composition (Fig. 3).

For the 80 V applied sample, the thickness of the anodic layer was measured at 463.0 nm composed of Fe and Cr-oxide. The porous structure of Cr-oxide was revealed in the TEM cross-sectional image. Lowering the voltage down to 60 V, a thin and compact alumina layer appeared in between of upper compact Fe-oxide and inner porous Cr-oxide, having a total thickness of approximately 663 nm. With a low voltage of 30 V, the main anodic layer was composed of a highly porous alumina layer on the top and a certain amount of Fe and Cr-oxide layer underneath (total thickness: 413.8 nm). Finally, with the lowest voltage applied sample (20 V), the anodic layer was mainly highly porous alumina with thin Fe and Cr-oxide layer beneath having a total thickness of 576.8 nm.

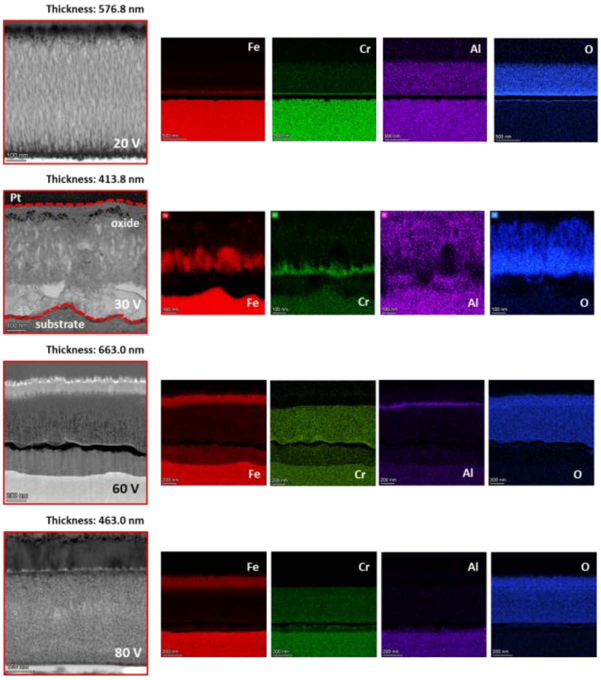

Fig. 3. Cross-sectional TEM images and EDS mappings of 20, 30, 60, and 80 V anodized FeCrAl alloy

As the oxide forming tendency of each main component in the FeCrAl alloy can be depicted as following Fig. 4(a), the oxide manipulating mechanism can be explained (Fig. 4(b)). For relatively low energy input, the oxidation tendency significantly affects the composition of the fabricated oxide layer. As you can see from Fig. 3, Al mainly forms the oxide layer owing to its high tendency of oxide formation in the 20 and 30 V applied samples. On the other hand, with relatively high energy input, the composition ratio in the alloy strongly affects the composition of the oxide. Because Fe is the base metal showing the highest composition ratio and the percentage of Cr is much higher compared to Al, over 60 V of energy input, the anodization provides mainly Fe and Cr oxide on the surface owing to their high composition ratio in the alloy. With such a mechanism, the input energy control successfully manipulated the composition of the fabricated oxide layer. Also, it was worthy to focus on the consistency of the porous structures of the samples having different applied potentials owing to the irrelevant effect of chemical dissolution reactions with electrochemical anodic formation reactions.

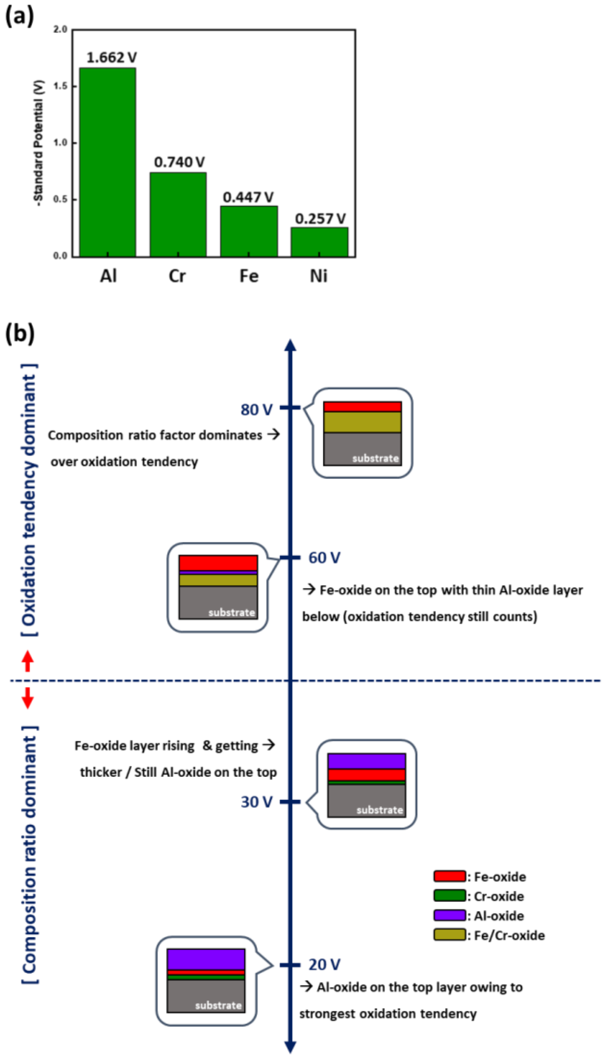

Fig. 4. (a) Oxidation tendency of Al, Cr, Fe, and Ni, (b) anodic layer manipulating mechanism

3.3 Selection of Corrosion Samples

The experiment's goal is to create a porous alumna that will transform the template into protective $MgAl_2O_4$ spinel oxide. The lower voltage applied samples, which are 20 and 30 V applied, demonstrated sufficient conditions for additional experimentation among the oxide composition modified samples (20 to 80 V applied). As previously stated, even at low energy input conditions, the strong oxidation tendency of Al produced those alumina-rich anodic layers. The XPS tool was used for depth profiling in order to look more closely at the anodic layer that was created on the two samples. Each sample's atomic percentages by depth direction revealed an anodic layer rich in alumina on the surface (Fig. 5). The 20 V applied sample displayed thicker and more stable alumina than the 30 V applied sample, which is consistent with the EDS mapping results in Fig. 3.

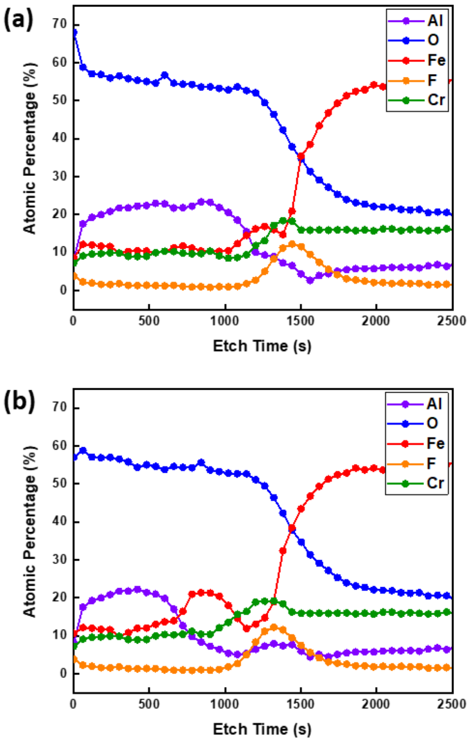

Fig. 5. XPS depth profiling of (a) 20 V and (b) 30 V applied anodization samples

3.4 Molten salt corrosion test

Anodized samples and bare FeCrAl alloy were used in the molten salt corrosion test, which was carried out at 600 °C. In order to compare the corrosion resistance by describing the surface and cross-sectional morphologies, the samples were first subjected to a 100 h molten salt corrosion technique (Fig.6).

As described in Fig. 6 (a), the surface of corroded bare FeCrAl alloy showed Mg-O corrosion products and grain boundary dissolution of Cr. The cross-sectional image showed 35.56 um of Cr-depletion thickness and Al_2O_3 precipitation in the depth direction. The 20 V applied anodization sample displayed uniform and stable Mg and Al-rich oxide on the surface having a thickness of approximately 1.81 um, in comparison to the bare FeCrAl alloy sample (Fig. 6(b)). When compared to the bare sample, the cross-sectional image revealed a substantially lower value of 7.78 um for the Cr-depletion thickness. The Cr-depletion thickness in the 30 V applied anodization sample was measured as 10.35 um, which is also better than in the bare sample. Nevertheless, a spallation area in the surface morphology caused substrate exposal. Because of its fast rate of dissolution in molten chloride salt environments, the thick Fe and Cr-oxide layer beneath the alumina layer, which can be seen from the TEM image (Fig. 3), may produce such spallation at the surface oxide layer [8]. Consequently, because of its greater stability, the 20 V applied sample was further evaluated alone even though the 30 V applied sample displayed improved behavior.

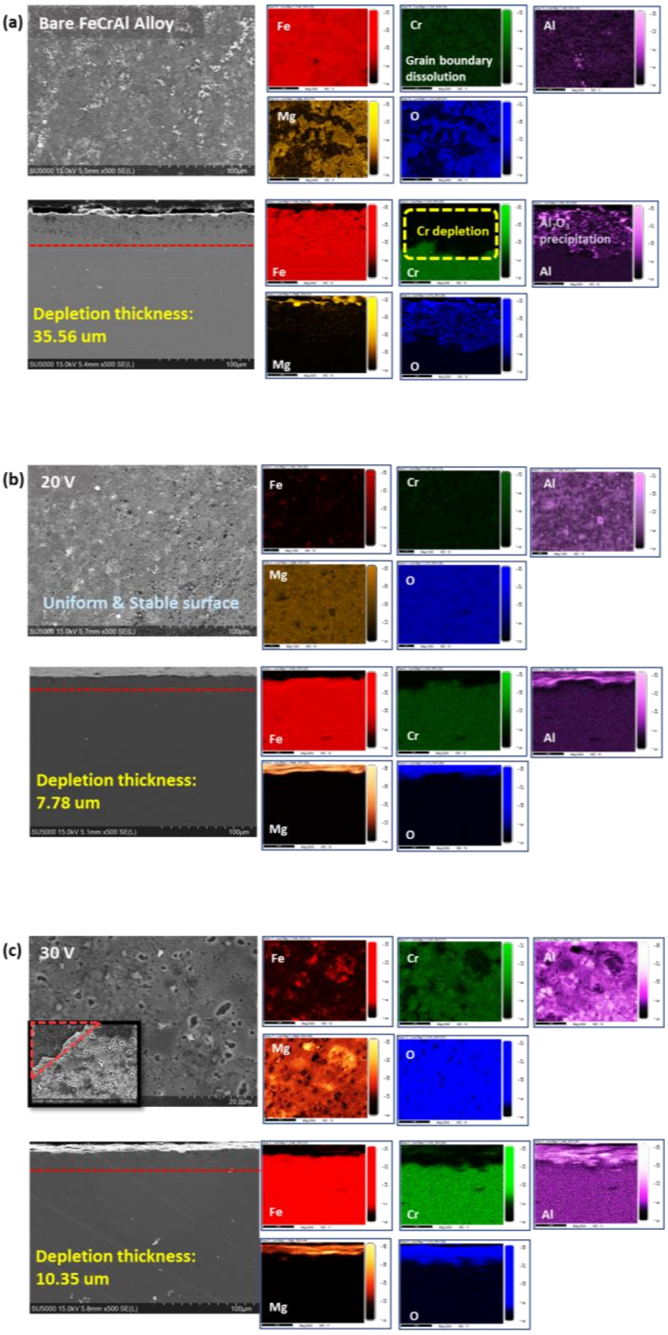

Fig. 6. Surface and cross-sectional SEM images of (a) bare FeCrAl alloy, (b) 20 V, and (c) 30 V anodized samples after 100 h corrosion test

Following the 100 h corrosion test, Fig. 7 shows the diffraction patterns of the corroded 20 V anodization sample and the corroded bare FeCrAl alloy for additional characterization. As stated, the anodized sample displayed alumina peaks alongside the substrate peak, but the bare FeCrAll alloy only displayed the substrate alloy peak prior to the corrosion test. The exceptional formation of α and θ phases of alumina in the anodized sample at a relatively lower temperature attributed to the high surface area of the porous structured template providing active transition sites and further inclusion of AlF_3 during the anodization process may lower the nucleation barrier of the stable phase [19,20]. The bare FeCrAl alloy then displayed MgO and Fe-doped MgO as corrosion products after the 100 h corrosion test. MgO and Fe-doped MgO were also found in the anodized sample, but the most important finding was the presence of $MgAl_2O_4$ spinel peaks that were in agreement with the EDS mapping results shown in Fig. 6(b).

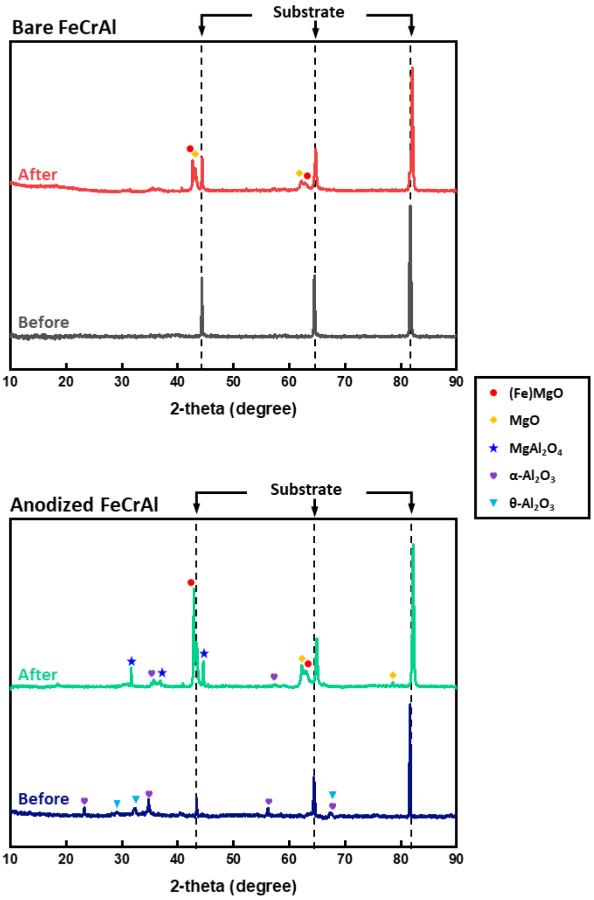

Fig. 7. Diffraction patterns of bare FeCrAl alloy and 20 V anodized sample before and after the 100 h corrosion test

Additional corrosion experiments were carried out using bare FeCrAl alloy and an anodization sample (20 V) in order to investigate deeper corrosion resistance characteristics. To compare the Cr-depletion thickness (the most important aspect in corrosion resistance comparisons), Fig. 8 shows the cross-sectional corrosion results of bare FeCrAl alloy after 300 and 500 h. The line scan in the depth direction revealed that the 300 h corroded sample had a Cr-depletion thickness of roughly 53.3 um. In the case of a 500 h corroded sample, the Cr-depletion thickness was measured as 85.76 um, far increased with increasing corrosion time.

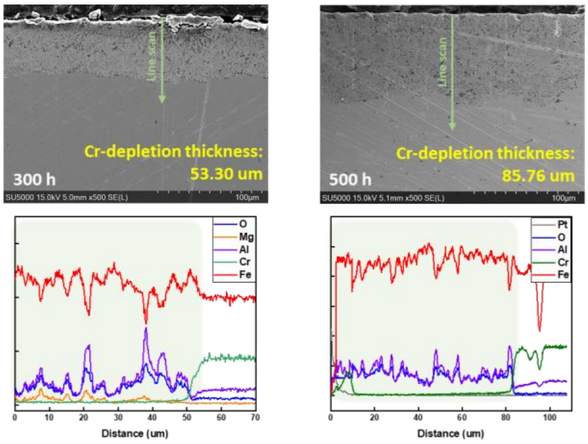

Fig. 8. Cr-depletion thickness of bare FeCrAl alloy after 300 and 500 h corrosion test using EDS line scan

Apart from those results, Fig. 9 depicts the corrosion results of 20 V anodization samples. Fig. 9 (a) showed a 300 h corroded anodization sample having 13.8 um of Cr-depletion thickness. The cross-sectional view revealed the compact and uniform $MgAl_2O_4$ spinel oxide layer on the surface having a thickness of 2.89 um. Further corrosion showed a slightly increased Cr-depletion thickness of 16.12 um, also resulting in a protective $MgAl_2O_4$ spinel oxide layer on the surface with 3.56 um thickness which is far grown than the 100 and 300 h corroded samples (Fig. 9 (b)). The important finding was that the anodized sample demonstrated significantly better corrosion resistance behavior in subsequent corrosion tests, exhibiting significantly reduced Cr-depletion thickness with a protective oxide layer on the surface.

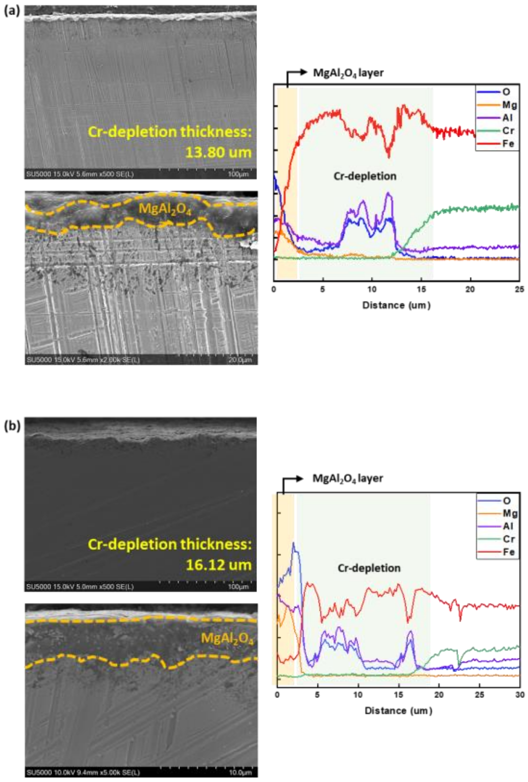

Fig. 9. Cr-depletion thickness of 20 V anodized sample after (a) 300 and (b) 500 h corrosion test using EDS line scan

3.5 Corrosion Protection Mechanism

The corrosion test of 100-500 h showed improvement in corrosion resistance of the anodized sample compared to bare FeCrAl alloy. The enhancement can be seen in the Cr-depletion thickness comparison data depicted in Fig. 10. In contrast to the bare FeCrAl alloy sample, which exhibits an exponential increase in Cr-depletion thickness, anodized samples exhibiting saturating behavior show significantly lower values.

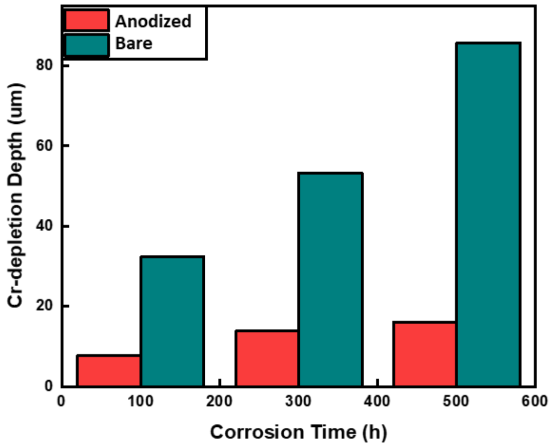

Fig. 10. Comparision in corrosion resistance behavior of bare FeCrAl alloy and anodized sample

Those improvements have been identified as a result of the $MgAl_2O_4$ protective layer on the surface of an anodized sample. In the earlier stage of the corrosion test, corrosive media penetrating through the porous alumina generates various corrosive species such as HCl, Cl_2, and etc. as shown in reaction (1-4)[8,21].

$$(1)\ MgCl_2 + H_2O \rightarrow MgOHCl + HCl$$

$$(2)\ MgOHCl \rightarrow MgOH^+ + Cl^-$$

$$(3)\ O_2 + 4Cl^- \rightarrow O^{2-} + 2Cl_2$$

$$(4)\ HCl + O_2 \rightarrow H_2O + 2Cl_2$$

After a certain amount of time, corrosive species eventually approach the beneath Fe and Cr-oxide dissolving them to generate additional oxygen sources. And, at the same time, MgO corrosion products are produced as a reaction (5). The porous alumina reacts with MgO and Mg^{2+} in the media to convert the template into a $MgAl_2O_4$ spinel oxide layer as a reaction(6)[9,14]. Owing to the porous structure of the alumina template, the volume expansion stress from the insertion of Mg^{2+} ions into the alumina lattice can be mitigated.

$$(5)\ MgCl_2 + H_2O \rightarrow MgO + 2HCl$$

$$(6)\ MgO + Al_2O_3 \rightarrow MgAl_2O_4$$

Further corrosion procedure accelerates the conversion of alumina into $MgAl_2O_4$ spinel providing sufficient reactants and kinetic energy resulting in a compact and protective oxide layer on the surface. With those protective spinel oxide layers having high chemical resistant characteristics, the FeCrAl alloy substrate can be defended against the aggressive molten chloride salt media. Diffusion of Mg and Al ions each from the outer media and inner substrate, combined with the oxygen sources from the dissolution of Fe and Cr-oxide, a thicker $MgAl_2O_4$ conversion layer was possible compared to the base alumina template.

4. Conclusion

This study significantly enhances the corrosion resistance of structural materials in molten chloride salt using electrochemical anodization. Instead of the alumina layer that inevitably leads to the formation of a $MgAl_2O_4$ layer, this research intentionally targets the direct formation of the $MgAl_2O_4$ layer on the surface at first. Whereas the conventional formation of $MgAl_2O_4$ results in an unstable structure due to volume expansion stress, this study selectively forms a porous alumina template by anodization, which mitigates the volume expansion stress during Mg ion insertion. As a result, a stable and protective $MgAl_2O_4$ spinel layer is successfully developed. Comparative corrosion tests conducted from 100 to 500 h showed significant improvements. For bare FeCrAl alloy structural materials, the Cr-depletion thickness increased exponentially, exhibiting 35.56, 53.30, and 85.76 µm. In contrast, the anodization sample exhibited significantly reduced values of 7.78, 13.80, and 16.12 µm. This novel approach leverages the Mg source in the molten salt environment to facilitate the formation of a protective oxide layer, turning a threatening challenge into an opportunity. These findings are expected to make substantial contributions to the commercialization of 4th generation nuclear reactors and various other fields utilizing molten salt media.

REFERENCES

[1] Guo, Shaoqiang, et al. "Corrosion in the molten fluoride and chloride salts and materials development for nuclear applications." Progress in Materials Science 97 (2018): 448-487.

[2] Roper, Robin, et al. "Molten salt for advanced energy applications: A review." Annals of Nuclear Energy 169 (2022): 108924.

[3] Mausolff, Zander, Mark DeHart, and Sedat Goluoglu. "Design and assessment of a molten chloride fast reactor." Nuclear Engineering and Design 379 (2021): 111181.

[4] Han, Dongmei, et al. "Enhanced corrosion resistance of alloy in molten chloride salts by adding nanoparticles for thermal energy storage applications." Journal of Energy Storage 64 (2023): 107172.

[5] Raiman, Stephen S., et al. "Amorphous and partially-amorphous metal coatings for corrosion resistance in molten chloride salt." Solar Energy Materials and Solar Cells 201 (2019): 110028.

[6] Wang, Chengxu, et al. "Corrosion behavior and elements interdiffusion between a Ni coating and GH3535 alloy with and without a CrN barrier in molten fluoride salts." Journal of Nuclear Materials 514 (2019): 348-357.

[7] Gomez-Vidal, J. C., et al. "Corrosion resistance of alumina-forming alloys against molten chlorides for energy production. I: Pre-oxidation treatment and isothermal corrosion tests." Solar Energy Materials and Solar Cells 166 (2017): 222-233.

[8] Ding, Wenjin, et al. "Molten chloride salts for next generation concentrated solar power plants: Mitigation strategies against corrosion of structural materials." Solar Energy Materials and Solar Cells 193 (2019): 298-313.

[9] Pellicot, Louis, et al. "Corrosion of a Nickel-Based Alumina-Forming Alloy in Molten NaCl–MgCl2 at 600° C For the Development of a Molten Salt Nuclear Reactor." High Temperature Corrosion of Materials 101.5 (2024): 1041-1054.

[10] Okonkwo, Bright O., et al. "Corrosion behaviour of Al-containing alloys in Cl-based molten salt environment." Journal of Nuclear Materials 599 (2024): 155207.

[11] Pellicot, Louis, et al. "Corrosion of Two Iron-Based Aluminaforming Alloys in NaCl-MgCl2 Molten Salts at 600° C." Materials 17.13 (2024): 3224.

[12] Wang, Liuxin, et al. "Corrosion behavior of aluminum-containing austenitic steels exposed to high-temperature molten chloride salt." Solar Energy Materials and Solar Cells 280 (2025): 113269.

[13] Wang, Mingliang, Yinong Liu, and Hong Yang. "A unified thermodynamic theory for the formation of anodized metal oxide structures." Electrochimica acta 62 (2012): 424-432.

[14] Kim, KeeHyun. "Formation of endogenous MgO and MgAl2O4 particles and their possibility of acting as substrate for heterogeneous nucleation of aluminum grains." Surface and Interface Analysis 47.4 (2015): 429-438.

[15] Zhao, Youyang, Noah Klammer, and Judith Vidal. "Purification strategy and effect of impurities on corrosivity of dehydrated carnallite for thermal solar applications." Rsc Advances 9.71 (2019): 41664-41671.

[16] Sulka, Grzegorz D. "Introduction to anodization of metals." Nanostructured Anodic Metal Oxides. Elsevier, 2020. 1-34.

[17] Sun, Yan, et al. "Influence of water content on the formation of TiO2 nanotubes and photoelectrochemical hydrogen generation." Journal of Alloys and Compounds 711 (2017): 514-520.

[18] Terashima, Ayasa, Mana Iwai, and Tatsuya Kikuchi. "Nanomorphological changes of anodic aluminum oxide fabricated by anodizing in various phosphate solutions over a wide pH range." Applied Surface Science 605 (2022): 154687.

[19] Carstens, Simon, Ralf Meyer, and Dirk Enke. "Towards macroporous α-Al2O3—Routes, possibilities and limitations." Materials 13.7 (2020): 1787.

[20] Shimbo, Mitsuo, et al. "Influence of addition of AlF3 on thermal decomposition of gibbsite and phase transition of the intermediate alumina to α-Al2O3." Journal of the Ceramic Society of Japan 115.1345 (2007): 536-540.

[21] Guo, Lili, et al. "Excellent corrosion resistance of 316 stainless steel in purified NaCl-MgCl2 eutectic salt at high temperature." Corrosion Science 166 (2020): 108473.